Ocean Surface Wave Optical Roughness – Analysis of Innovative Measurements

Michael L. Banner
School of Mathematics and Statistics
The University of New South Wales
Sydney 2052, Australia
Tel : (+61-2) 9385-7071 fax: (+61-2) 9385-7123 email: m.banner@unsw.edu.au

Russel P. Morison
School of Mathematics and Statistics
The University of New South Wales
Sydney 2052, Australia
Tel : (+61-2) 9385-7064 fax: (+61-2) 9385-7123 email: r.morison@unsw.edu.au

Award Number: N00014-11-1-0054

LONG-TERM GOALS

We are part of a multi-institutional research team funded by the ONR-sponsored Radiance in a Dynamic Ocean (RaDyO) program. The primary research goals of the program are to (1) examine time-dependent oceanic radiance distribution in relation to dynamic surface boundary layer (SBL) processes; (2) construct a radiance-based SBL model; (3) validate the model with field observations; and (4) investigate the feasibility of inverting the model to yield SBL conditions. Our goals are to contribute innovative measurements, analyses and models of the sea surface roughness at length scales as small as a millimeter. This characterization includes microscale and whitecap breaking waves.

The members of the research team are

Michael Banner, School of Mathematics, UNSW, Sydney, Australia

Johannes Gemmrich, Physics and Astronomy, UVic, Victoria, Canada

Russel Morison, School of Mathematics, UNSW, Sydney, Australia

Howard Schultz, Computer Vision Laboratory, Computer Science Dept, U. Mass., Mass

Christopher Zappa, Lamont Doherty Earth Observatory, Palisades, NY

OBJECTIVES

Nonlinear interfacial roughness elements - sharp crested waves, breaking waves as well as the foam, subsurface bubbles and spray they produce, contribute substantially to the distortion of the optical transmission through the air-sea interface. These common surface roughness features occur on a wide range of length scales, from the dominant sea state down to capillary waves. Wave breaking signatures range from large whitecaps with their residual passive foam, down to the ubiquitous centimeter scale microscale breakers that do not entrain air. There is substantial complexity in the local wind-driven sea

Report Documentation Page

Form Approved
OMB No. 0704-0188

1. REPORT DATE	2. REPORT TYPE	3. DATES COVERED
30 SEP 2013		**00-00-2013 to 00-00-2013**

4. TITLE AND SUBTITLE	5a. CONTRACT NUMBER
Ocean Surface Wave Optical Roughness - Analysis of Innovative Measurements	5b. GRANT NUMBER
	5c. PROGRAM ELEMENT NUMBER
6. AUTHOR(S)	5d. PROJECT NUMBER
	5e. TASK NUMBER
	5f. WORK UNIT NUMBER
7. PERFORMING ORGANIZATION NAME(S) AND ADDRESS(ES) **The University of New South Wales,School of Mathematics and Statistics,Sydney 2052, Australia,**	8. PERFORMING ORGANIZATION REPORT NUMBER
9. SPONSORING/MONITORING AGENCY NAME(S) AND ADDRESS(ES)	10. SPONSOR/MONITOR'S ACRONYM(S)
	11. SPONSOR/MONITOR'S REPORT NUMBER(S)

12. DISTRIBUTION/AVAILABILITY STATEMENT
Approved for public release; distribution unlimited

13. SUPPLEMENTARY NOTES

14. ABSTRACT

15. SUBJECT TERMS

16. SECURITY CLASSIFICATION OF:			17. LIMITATION OF ABSTRACT	18. NUMBER OF PAGES	19a. NAME OF RESPONSIBLE PERSON
a. REPORT **unclassified**	b. ABSTRACT **unclassified**	c. THIS PAGE **unclassified**	**Same as Report (SAR)**	**8**	

surface roughness microstructure, including very steep nonlinear wavelets and breakers. Traditional descriptors of sea surface roughness are scale-integrated statistical properties, such as significant wave height, mean squared slope [e.g., *Cox and Munk*, 1954a] and breaking probability [e.g., *Holthuijsen and Herbers*, 1986]. Subsequently, spectral characterisations of wave height, slope and curvature have been measured, providing a scale resolution into Fourier modes for these geometrical sea roughness parameters. More recently, measurements of whitecap crest length spectral density [e.g., *Gemmrich et al.*, 2008; *Phillips et al.*, 2001] and microscale breaker crest length spectral density [e.g., *Jessup and Phadnis*, 2005] have been reported.

Our effort seeks to provide a more comprehensive description of the physical and optical roughness of the sea surface. We will achieve this through the analysis of our suite of comprehensive sea surface roughness observational measurements within the RADYO field program. These measurements are designed to provide optimal coverage of fundamental optical distortion processes associated with the air-sea interface. In our data analysis, and complementary collaborative effort with RaDyO modelers, we are investigating both spectral and phase-resolved perspectives. These will allow refining the representation of surface wave distortion in present air-sea interfacial optical transmission models.

APPROACH

We build substantially on our accumulated expertise in sea surface processes and air-sea interaction. We are working within the larger team (listed above) measuring and characterizing the surface roughness. This team is contributing the following components to the primary sea surface roughness data gathering effort in RaDyO:

- polarization camera measurements of the sea surface slope topography, down to capillary wave scales, of an approximately 1m x 1m patch of the sea surface (see Figure 1), captured at video rates. [Schultz, Zappa]
- co-located and synchronous orthogonal 75 Hz linear scanning laser altimeter data to provide spatio-temporal properties of the wave height field (resolved to O(0.5m) wavelengths) [Banner, Morison]
- high resolution video imagery to record whitecap data from two cameras, close range and broad field [Gemmrich]
- fast response, infrared imagery to quantify properties of the microscale breakers, and surface layer kinematics and vorticity [Zappa]
- air-sea flux package including sonic anemometer to characterize the near-surface wind speed and wind stress [Zappa]

The team's envisaged data analysis effort includes: detailed analyses of the slope field topography, including mean square slope, skewness and kurtosis; laser altimeter wave height and large scale wave slope data; statistical distributions of whitecap crest length density in different scale bands of propagation speed and similarly for the microscale breakers, as functions of the wind speed/stress and the underlying dominant sea state. Our contributions to the modeling effort will focus on using RaDyO data to refine the sea surface roughness transfer function. This includes the representation of nonlinearity and breaking surface wave effects including bubbles, passive foam, active whitecap cover and spray, as well as micro-breakers.

WORK COMPLETED

Our effort in FY13 comprised further collaborative analysis of the sea surface roughness measurements gathered from FLIP during the RaDyO field experiments in the Santa Barbara channel during Sept. 5-27, 2008 and Hawaii during Aug. 23-Sept.v16, 2009. We participated actively in extending our analysis and validation of the polarimetric and wave breaking data.

One is in press [Gemmrich et al., 2013] and one is in revision [Banner et al., 2013].

RESULTS

To provide the context of our new results for FY13, during the SBC experiment, diurnal processes were the origin of most of the variability in the atmospheric and oceanic forcing. The momentum, sensible heat and latent heat fluxes all show a diurnal cycle similar to the wind speed. In strong contrast, in the HI experiment, processes were driven by the persistent easterly trade winds. This overview of the background air-sea flux conditions was obtained from time series of momentum (wind stress), sensible heat, and water vapor direct covariance fluxes during the Santa Barbara Channel (hereafter SBC) and central Pacific Ocean studies of Hawaii (hereafter HI). Full details are provided in *Zappa et al.* [2012] and *Dickey et al.* [2012].

In response to the growing need for robust validation data for the Phillips (1985) breaking wave spectral framework, we contribute new field results observed from R/P FLIP for the breaking crest length distributions during two different wind-wave conditions, and breaking strength during one wind-wave condition. According to Phillips (1985), the scale of each breaking front wave is associated with the phase speed of the underlying wave that is breaking, and the associated width of the breaking front contributes at that scale to the distribution of mean breaking crest width/unit sea surface area, $\Lambda(c)$. Here we characterize each breaking front velocity by its initial observed velocity $\mathbf{c}_b$, where $c_b=\alpha c$, where $\alpha\sim0.8$, and define the azimuthally integrated crest length distribution of measured $\Lambda(c_b)$. Then, according to Phillips (1985) breaking wave spectral framework, the spectral distribution of wave energy dissipation rate $\varepsilon(c_b)$ is given by $\varepsilon(c_b) = b(c_b)\,\rho\, g^{-1}\, c_b^{-5}\, \Lambda(c_b)$, where $b(c_b)$ is the scale dependent breaking strength coefficient that links the breaker front kinematics to the energetics and dynamics of the breaking waves. The water density is ρ and g is the gravitational acceleration.

Breaking crest length distributions

The first experiment in the SBC had developing seas and the second experiment near HI had mature seas. These are amongst the first experiments to use dissipation rate measurements probing up into the breaking crest together with simultaneous measurements of breaking crest length distributions. Of particular interest is that the dynamic range of the wind stress is larger during the SBC experiment than the Hawaii experiment. Together these two experiments provide wave breaking measurements over an interesting dynamic range of wind speeds spanning light and variable to strong.

Results on the breaking crest length distribution $\Lambda(c_b)$ for the two experiments are given in Fig. 2. A key feature of all observed $\Lambda(c_b)$ distributions at both experimental sites is a maximum at short-to-intermediate wave scales. The location of this maximum, which specifies the scale of the largest contribution of breaking crests, increases with wave age, however there is no clear dependence on wave age of the magnitude of this maximum. Wind speed and wave field parameters covered a much

broader range during the Santa Barbara Channel experiment compared to the experiment in the central Pacific Ocean south of Hawaii. These differences in the dynamic range of forcing parameters are directly reflected in the dynamic range of the breaking crest length distributions. At intermediate scales, i.e. 3 m/s $\leq c_b \leq$ 5 m/s, the $\Lambda(c_b)$ distributions span almost two orders of magnitude in SBC, but only a factor O(5) in HI. The maximum levels of $\Lambda(c_b)$ are comparable between the two experiments, but the overall mean level of $\Lambda(c_b)$ is larger in HI. It is seen that the slope of the $\Lambda(c_b)$ curves for higher c_b values fluctuates about the Phillips (1985) canonical form $\Lambda(c_b) \sim c_b^{-6}$, which is discussed further below.

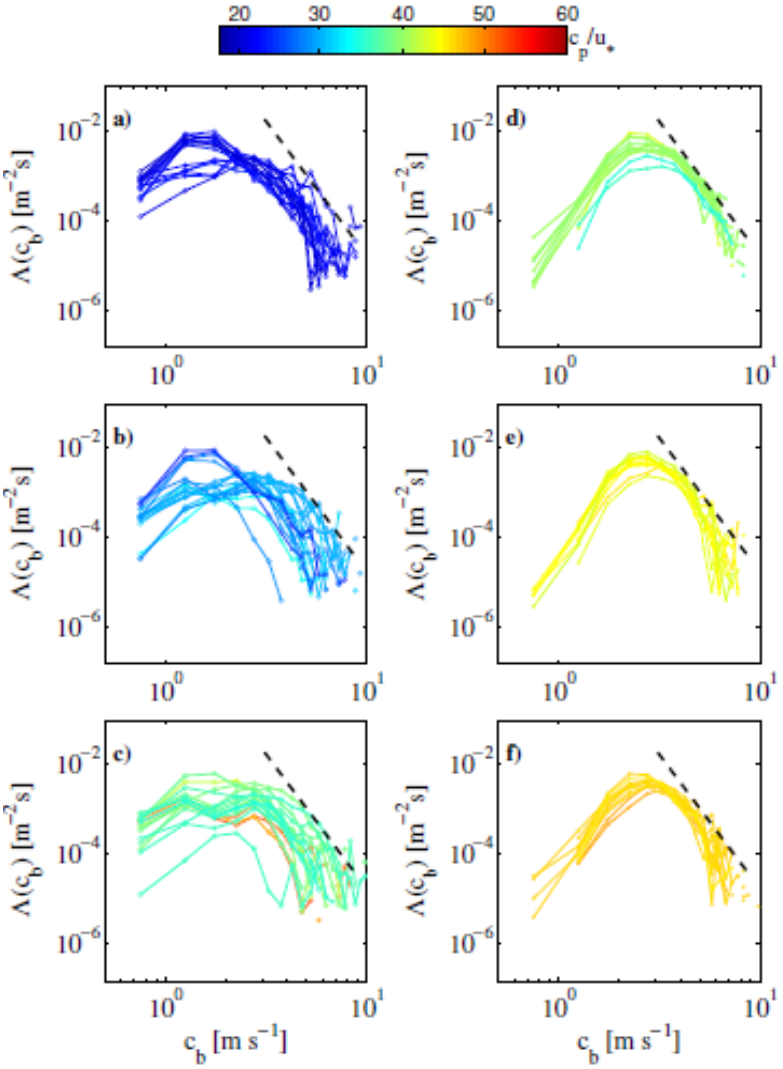

Figure 2. Distributions of spectral breaking crest length per unit area, $\Lambda(c_b)$, against observed breaker speed c_b during the experiments in Santa Barbara Channel (a-c) and Hawaii (d-f). Colors represent wave age c_p/u_*. The dashed line indicates the m = -6 slope predicted by Phillips (1985). For each experiment, data runs are split into 3 equal-sized sub-panels, covering the wave age sub-ranges during the entire data sets.

There are some noteworthy differences in the shape of breaking crest length distributions of the two data sets, likely associated with different development stages of the wave field. We calculated overall mean distributions from 24 SBC runs with $c_p/u_* \leq 25$, characterizing growing seas, and from 14 HI runs with $c_p/u_* \geq 45$, characterizing mature seas. These are shown in the left panel of Fig.3. There were no comparably mature sea states from the SBC data set to include. In growing seas, breaking spans the entire spectrum from dominant waves to scales associated with $0.1c_p$, where c_p is the speed of the spectral peak waves, whereas in mature seas no breaking is observed at scales larger than those corresponding to $0.6c_p$.

The normalized fifth moment of the breaking crest length distributions is shown in the right panel of Fig. 3. The fifth moment of the $\Lambda(c_b)$ distribution is related to the spectral energy dissipation rate. The strongest dissipation rate is seen to occur at small-to-intermediate scales in the mature sea, but at the large wave scale in the developing sea. Thus the velocity scale of the peak of the breaking dissipation rate decreases with increasing wave age. Despite the breaking in mature seas occurring over a smaller spectral bandwidth than in growing seas, the total dissipation rate in the mature seas is about three times higher. This is attributed to higher energy and momentum fluxes from the wind in HI.

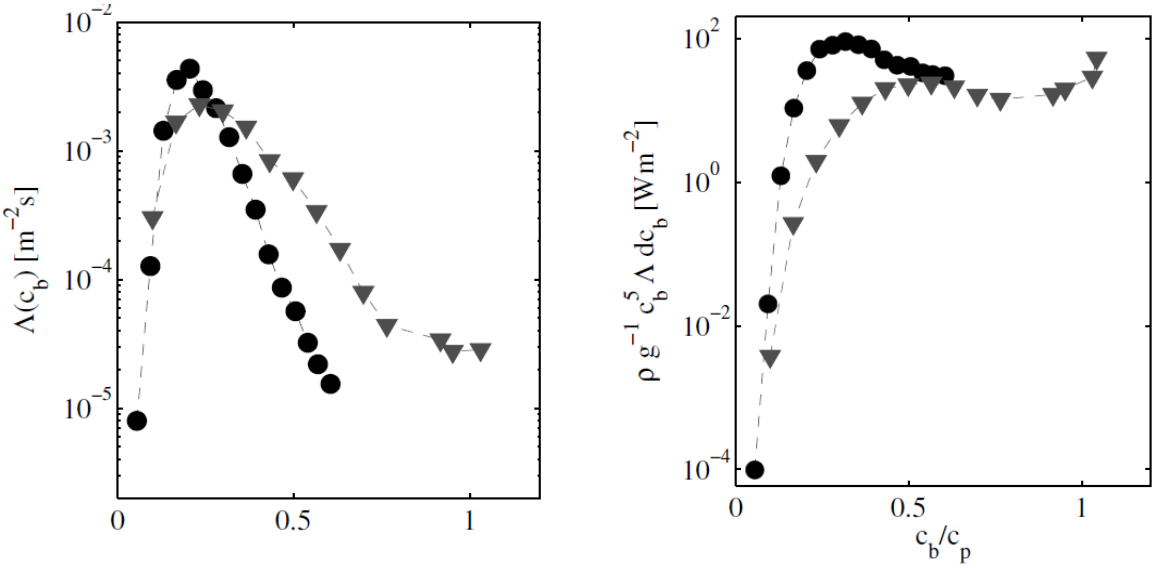

Figure 3. Overall mean breaking crest length distributions (left panel) and their 5th moment (right panel), for subsets of the data representing developing seas (gray triangles) and mature seas (black circles).

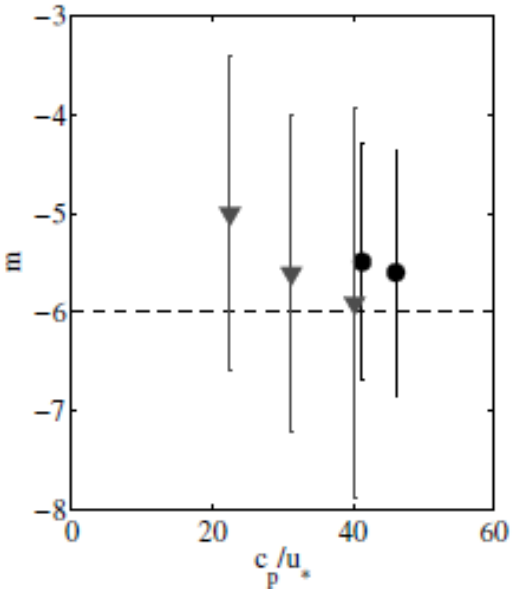

Figure 4. Bin-averaged exponent m (slope) of the breaking crest length distribution as function of wave age (c_p/u_*) for the Santa Barbara channel (gray triangles) and Hawaii experiment (black circles). The dashed line depicts the classical Phillips (1985) result m=-6. The vertical bars indicate ±1 standard deviation.

Further, in Fig. 4, it is seen that the breaking crest length spectrum tends to fall off more slowly than the c^{-6} behavior predicted by Phillips (1985). This result was statistically significant at the 95% confidence level. We note that this conclusion is weakly sensitive to the data processing methodology used, as discussed below.

Breaking strength parameter b

We note that the transition from the kinematic quantity of the crest length distribution to the dynamics of energy dissipation rate requires knowledge of the breaking strength parameter b. Estimates of the spectrally-resolved breaking parameter are only starting to become available and all previous studies based on field data report the scale-integrated value b_{eff}. Reported values of b_{eff} from different experiments span more than 3 orders of magnitude between these experiments, from $3x10^{-5}$ to $7x10^{-2}$ (Melville and Matusov, 2002; Gemmrich et al., 2008; Thomson et al., 2009). Recent work by Romero et al. (2012) suggests that approximating $b(c_b)$ by a uniform level, independent of c_b, is a reasonable approach, at least for wave scales shorter than the dominant waves. In any event, from our direct measurements of $\Lambda(c_b)$ and surface-piercing dissipation rates in the mature wind seas off HI, we directly measured the effective breaking strength parameter b_{eff} to be $4.2 \pm 1.8 \times 10^{-5}$ for the wave age (c_p/u_*) range of 40-47.

Sensitivity to data analysis methodology

In view of the rather large scatter in b_{eff} reported by different investigators pointed out above, we revisited the sensitivity of the whitecap analysis methodology. While there are differences in the detailed measurement of the individual breaker geometry, a significant source of variation arises because some investigators have chosen to partition the time-dependent geometry of each breaker into

variable speed bins as the breaker slows down, while other investigators, including ourselves, assign the mean crest length of a given breaker to its initial speed, as envisaged by Phillips (1985). The variable speed allocation method has the effect of aliasing $\Lambda(c_b)$ to slower waves, thereby increasing the exponent –m. Our analysis based on the RaDyO data sets estimates this difference at O(0.3 to 0.4). The corresponding impact on b_{eff} for the RaDyO data was a factor of O(2) increase associated with the variable speed method. We are investigating other possible sources that may be contributing to the large dynamic range of reported b_{eff} values.

IMPACT/APPLICATIONS

This effort will contribute a more detailed characterization of the wind driven air-sea interface, including wave breaking (whitecaps and microscale breaking). This is needed to provide more complete parameterizations of these processes, which will improve the accuracy of ocean optical radiative transfer models and trans-interfacial image reconstruction techniques.

REFERENCES

Cox, C., and W. Munk (1954a), Measurement of the roughness of the sea surface from photographs of the sun's glitter, *Journal of the Optical Society of America*, *44*(11), 838-850.

Dickey, T., et al. (2012), Introduction to special section on Recent advances in the study of optical variability in the near-surface and upper ocean, *Journal of Geophysical Research – Oceans*, *117*(C00H20), doi:10.1029/2012JC007964.

Fairall, C. W., E. F. Bradley, J. E. Hare, A. A. Grachev, and J. B. Edson (2003), Bulk parameterization of air-sea fluxes: Updates and verification for the COARE algorithm, *J. Climate*, *16*, 571-591.

Gemmrich, J. R., M. L. Banner, and C. Garrett (2008), Spectrally resolved energy dissipation and momentum flux of breaking waves, *J. Phys. Oceanogr.*, *38*, 1296-1312.

Holthuijsen, L. H., and T. H. C. Herbers (1986), Statistics of breaking waves observed as whitecaps in the open sea, *Journal of Physical Oceanography*, *16*, 290-297.

Jessup, A. T., and K. R. Phadnis (2005), Measurement of the geometric and kinematic properties of microsacle breaking waves from infrared imagery using a PIV algorithm, *Meas. Sci. Technol.*, *16*, 1961-1969.

Melville W.K., and P. Matusov P. (2002), Distribution of breaking waves at the ocean surface. *Nature* 417:58–63

Phillips, O.M. (1985), Spectral and statistical properties of the equilibrium range in wind-generated gravity waves, *Journal of Fluid Mechanics*, *156*, 505-531.

Phillips, O.M., F.L. Posner, and J.P. Hanson (2001), High resolution radar measurements of the speed distribution of breaking events in wind-generated ocean waves: surface impulse and wave energy dissipation rates, *J. Phys. Oceanogr.*, *31*, 450–460.

Romero, L., W.K. Melville, and J. Kleiss (2012), Spectral energy dissipation due to surface-wave breaking, *J. Phys. Oceanogr.*, doi:10.1175/JPO-D-1111-1072.1171,

Thomson, J., and A. Jessup (2009), A Fourier-based method for the distribution of breaking crests from video observations, *J. Atmos. Oceanic Technol.*, *26*, 1663-1671.

Zappa, C. J., J. R. Gemmrich, R. P. Morison, H. Schultz, M. L. Banner, D. A. LeBel, and T. Dickey (2012), An overview of sea state conditions and air-sea fluxes during RaDyO, J. Geophys. Res. Oceans, *117*, doi:10.1029/2011JC007336.

PUBLICATIONS

Gemmrich, J.R., C.J. Zappa, M.L. Banner and R.P. Morison, (2013). Wave breaking in developing and mature seas. J. Geophys. Res. Oceans, doi: 10.1002/jgrc.20334. [published, refereed].

Banner, M.L., C.J. Zappa and J.R. Gemmrich (2013). A note on Phillips spectral framework for ocean whitecaps. J. Phys. Oceanogr. [in revision, refereed]

Zappa, C.J., J.R. Gemmrich, R.P. Morison, H. Schultz, M.L. Banner, D.A. LeBel, and T. Dickey (2012), An overview of sea state conditions and air-sea fluxes during RaDyO, J. Geophys. Res. Oceans, 117, doi:10.1029/2011JC007336. [published, refereed].

Zappa, C.J., M.L. Banner, H. Schultz, A. Corrada-Emmanuel, L.B. Wolff, and J. Yalcin (2008), Retrieval of short ocean wave slope using polarimetric imaging, Measurement Science and Technology, 19(055503), doi:10.1088/0957-0233/1019/1085/055503. [published, refereed].